A numerical study of gravity waves induced by convection associated with Typhoon Rusa

S.-Y. Kim and H.-Y. Chun

Department of Atmospheric Sciences, Yonsei University, Seoul, Korea

J.-J. Baik

School of Earth and Environmental Sciences, Seoul National University, Seoul, Korea

Received 15 September 2005; revised 30 October 2005; accepted 15 November 2005; published 30 December 2005.

[1] Typhoon Rusa (2002) is simulated using a three-dimensional mesoscale model (MM5), and the characteristics of gravity waves generated by convection associated with the typhoon are investigated. The gravity waves in the stratosphere propagate in two directions, northwestward and southeastward according to the convective bands propagating in the same directions, although the typhoon itself moves north-northeastward. Spectral analyses show that the inertio-gravity waves (IGWs) in the stratosphere generated by Rusa have a dominant horizontal wavelength of 300–600 km, a vertical wavelength of 3–11 km, and a period of 6–11 hrs. A large fraction of the IGWs is filtered out in the upper troposphere and stratosphere mainly due to the critical-level filtering process. The decreased magnitude of the momentum flux with height in a non-filtered region is likely due to the damping process, with a minor contribution by the wave breaking process that can occur exclusively near the critical-level phase speeds. **Citation:** Kim, S.-Y., H.-Y. Chun, and J.-J. Baik (2005), A numerical study of gravity waves induced by convection associated with Typhoon Rusa, *Geophys. Res. Lett.*, *32*, L24816, doi:10.1029/2005GL024662.

1. Introduction

[2] Recently, the importance of cumulus convection as a source of non-stationary gravity waves has been identified. Convectively generated gravity waves have been observed [e.g., *Pfister et al.*, 1993; *Dewan et al.*, 1998] and numerically simulated using mesoscale models [e.g., *Alexander and Holton*, 1997; *Piani et al.*, 2000; *Lane et al.*, 2001; *Horinouchi et al.*, 2002; *Song et al.*, 2003], and their characteristics and generation mechanisms have been investigated. Vertically propagating convective gravity waves with a wide phase-speed spectrum are known to play an important role in maintaining the zonal-mean zonal wind in the tropics, such as quasi-biennial oscillation (QBO) [*Alexander and Holton*, 1997; *Sato and Dunkerton*, 1997], and in the extratropical regions [*Chun et al.*, 2004]. However, most of the observational and numerical modeling studies of convective gravity waves have been conducted in the tropics, with little attention given to the middle latitudes.

[3] Among the various types of convective systems, typhoon is perhaps the most well-organized and vigorous convective system. Gravity waves generated by typhoons have been observed by radar and windsondes [e.g., *Sato*, 1993; *Chane-Ming et al.*, 2002; *Dhaka et al.*, 2003], and their characteristics on the horizontal (ranging from 50 to 2000 km) and vertical wavelengths (ranging from 1.5 to 6 km) and periods (ranging from 60 min to 1.6 day) differ significantly depending on the individual cases and observation method.

[4] Observational studies are not sufficient to understand the characteristics of gravity waves generated by typhoons. Hence, appropriate numerical simulations are needed. Only recently, Z. Chen et al. (Gravity waves generated by a tropical cyclone-A numerical simulation study, submitted to Journal of Geophysical Research, 2005, hereinafter referred to as Chen et al., submitted manuscript, 2005) used a mesoscale model to examine gravity waves generated by typhoon Winnie. They found that the typhoon-induced gravity waves have a horizontal wavelength of 500–1000 km and a period of 10–15 hrs, and they suggested that the vertically decreasing wave momentum flux is mainly due to the damping process.

[5] In this study, we simulate typhoon Rusa, which passed through the Korean peninsula in 2002, using a three-dimensional mesoscale model, and the characteristics of gravity waves associated with the typhoon are investigated by spectral analyses of wind and temperature perturbations and momentum flux. The wave propagation mechanism is examined by comparing the convective source with induced wave spectra.

2. Numerical Experiment

[6] The numerical model used in this study is the Fifth-Generation Pennsylvania State University/National Center for Atmospheric Research (PSU/NCAR) Mesoscale Model (MM5) version 3 [*Dudhia et al.*, 2003]. A three-dimensional simulation is conducted with a horizontal grid spacing of 27 km. The horizontal domain has 145 × 145 grid points, with its center at 33.3°N and 127.2°E. 71 sigma levels are used (approximate vertical grid spacing of 500 m) from the surface to 10 hPa. For cloud physical processes, the cumulus parameterization by *Kain and Fritsch* [1993] and the simple-ice type microphysics scheme by *Dudhia* [1989] are used. For initial and boundary conditions, European Center for Medium-Range Weather Forecasts (ECMWF) reanalysis data with a horizontal resolution of 1.125° × 1.125° are used. The model is integrated for 36 hrs from 06 UTC 30 to 18 UTC 31 August 2002. For more realistic typhoon

0094-8276/05/2005GL024662$05.00

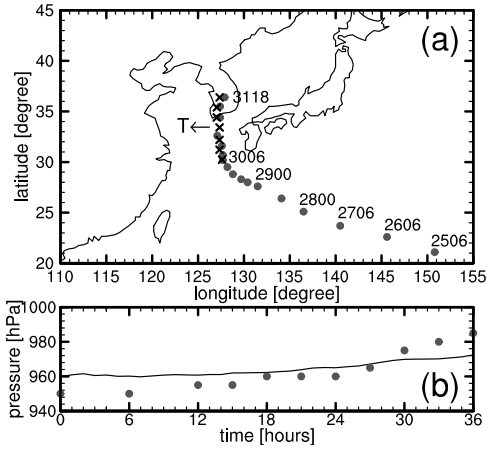

Figure 1. (a) Typhoon track and (b) minimum sea-level pressure. Filled circles indicate observed values, and crosses in Figure 1a and solid line in Figure 1b indicate simulated ones. Numbers in Figure 1a denote the time in days (first two digits) and UTC (last two digits). T denotes the time corresponding to Figure 2.

simulation, the Geophysical Fluid Dynamics Laboratory (GFDL) bogussing algorithm [*Kwon et al.*, 2002] is used.

[7] Figure 1 shows observed and simulated typhoon tracks near the Korean peninsula and minimum sea-level pressure. Rusa formed on 23 August and moved northwestward until it changed its direction to the north at 06 UTC 30 (start time of model integration). After landing on the Korean peninsula, Rusa moved north-northeastward. The model simulates the observed track fairly well although the simulated track shifts slightly to the west after landfall. At the beginning of the simulation, the minimum sea-level pressure is 960 hPa, somewhat higher than the observed value (950 hPa), and it rises up to about 972 hPa after 36 hrs. After Rusa landed on the Korean peninsula, the observed minimum sea-level pressure increased quickly up to 985 hPa, while the simulated one gradually increases with time. Given that the convective system and rainbands associated with the typhoon are reasonably well simulated compared with satellite images (not shown), along with typhoon track and intensity (Figure 1), we consider the present simulation is reasonably good to study typhoon-induced gravity waves.

3. Results

[8] Wave analysis is conducted using the vertical velocity and temperature data above z = 17 km. Figure 2 shows the vertical velocity and potential temperature at z = 21 km and their vertical cross section at y = 2808 km at t = 18 hr (corresponds to 00 UTC 31 August). Typhoon location at this time is marked by T in Figure 1a. In the horizontal cross section at z = 21 km, large amplitudes of vertical velocity and potential temperature appear in the northwestern part of the typhoon center, and this pattern propagates northwestward following the passage of the typhoon that moves north-northeastward, as shown in Figure 1a. In the southeastern region of the model domain, large amplitude of vertical velocity with small horizontal scales appears. This is mainly due to small-scale convective cells within the southeastern branch of typhoon-generated cloud bands. The domains enclosed by thick solid lines indicate the areas (domains A and B) of wave analysis, which will be presented in Figures 3 and 4.

[9] In the x-z cross-section of the vertical wind and potential temperature fields in the stratosphere, westward and upward propagation of wave perturbations is clearly seen. There exists a nearly 90° phase difference between the two variables, and this can be demonstrated quantitatively by calculating a lag correlation between the two variables and the power spectral density (PSD) of each variable with respect to zonal wavelength. For example, at z = 20 km, the dominant zonal wavelength of the vertical velocity and potential temperature is 324 km in their PSDs, and the lag-correlation coefficient between the two variables shows its minimum value of −0.667 at 81 km and its maximum value of 0.743 at 243 km. Given that 81 km and 243 km are 1/4 and 3/4 of the dominant horizontal wavelength (324 km),

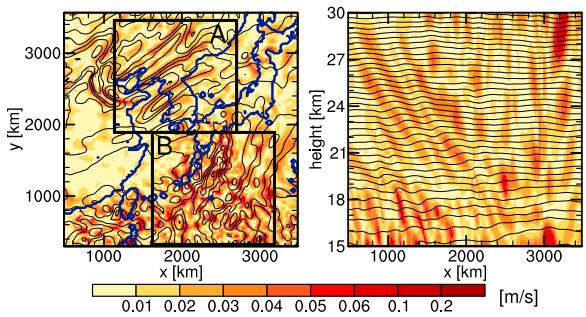

Figure 2. Magnitude of the vertical velocity (shaded) and potential temperature (contoured) (left) at z = 21 km and (right) their vertical cross section at y = 2808 km at t = 18 hr (corresponding to 00 UTC 31). Boxes in the left panel indicate domains where gravity wave analysis is conducted.

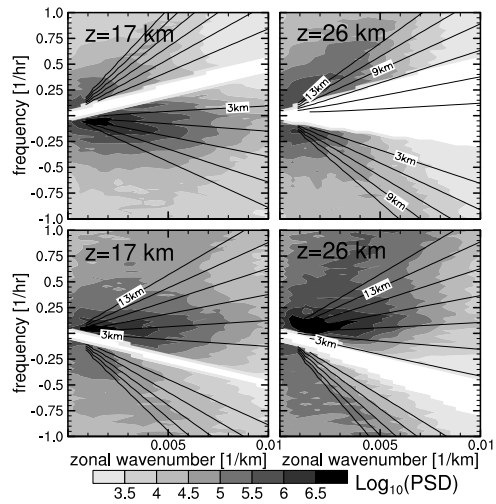

Figure 3. Base-10 logarithm of two-dimensional PSDs of vertical velocity as a function of zonal wave number and frequency at (left) z = 17 and (right) 26 km in (top) domain A and (bottom) domain B. The straight lines denote the vertical wavelength of IGWs.

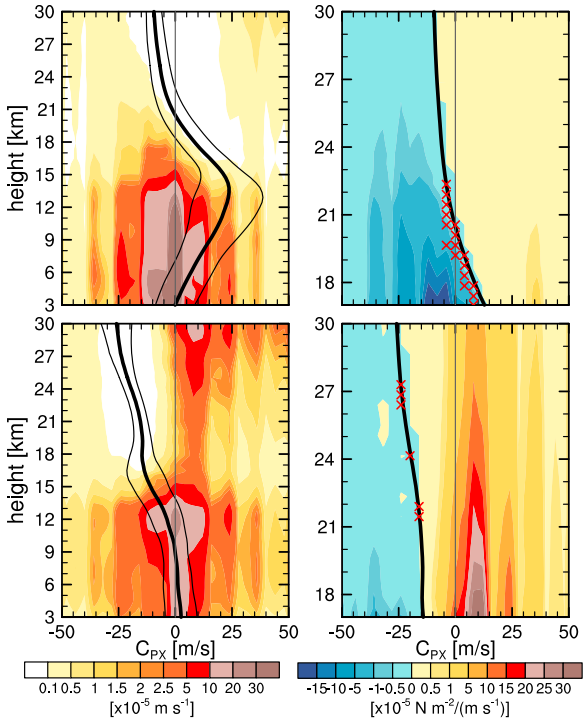

Figure 4. Profiles of the (left) vertical velocity spectrum from z = 3 to 30 km and (right) zonal momentum flux spectrum in the stratosphere as a function of zonal phase speed in (top) domain A and (bottom) domain B. Thick solid lines denote the time-mean of the basic-state wind (U) and thin solid lines in the left panels denote $U \pm \sigma$ (where σ is the standard deviation of U). The crosses in the right panels denote potential wave breaking regions.

respectively, the vertical velocity and potential temperature at z = 20 km can be considered as gravity waves. Similar results are also found at different heights and times and in domain B.

3.1. Characteristics of IGWs Generated by Typhoon

[10] To understand the characteristics of gravity waves quantitatively, we first extract the gravity wave component from the wind and temperature fields that satisfy the vertical propagation condition of IGWs ($f < \hat{\omega} < N$), where $\hat{\omega}$ is the intrinsic frequency, f is the Coriolis parameter, and N is the Brunt-Vaisala frequency. For this, time series of the wind and temperature (t = 1–36 hrs with a time interval of 300 s) are used in the wave-analysis domains shown in Figure 2. For calculating intrinsic frequency, horizontally averaged zonal wind at each time is used for the background wind.

[11] Figure 3 shows the PSD of the vertical velocity as a function of zonal wave number (k) and frequency relative to the ground (ω). The positive (negative) frequency denotes eastward (westward) propagation. In the spectral domain (k, ω), the white area denotes a wave-prohibition region, which is enclosed by two zonal phase speeds (slope in k-ω domain) that equal the minimum and maximum of the background wind in a target-height (wave-propagation height) range with the intercepts of $\omega = -f$ and $+f$. The average value of f in the wave-analysis domain is used for the calculation. Since the target-height range in the present study is from z = 17 to 30 km, the wave-prohibition areas shown in Figure 3 gradually widen with height. The straight lines in Figure 3 denote the vertical wavelength of IGWs calculated using the dispersion relation. In domain A, at z = 17 km, a large value for PSD is shown in the westward-propagating components of gravity waves with zonal wavelengths larger than about 220 km (wave number of 0.0045 km^{-1}) and periods longer than about 6 hrs (frequency of 0.16 hr^{-1}). Note that 220 km is about 8Δx, where Δx is the horizontal grid spacing (27 km). The vertical wavelength in this strong wave activity region ranges from 3 to 9 km. The eastward-propagating waves with similar zonal wavelengths and periods are mostly filtered out by the positive background wind in the upper troposphere. From z = 17 to 26 km, large fractions of the eastward-propagating components with near-stationary phase speeds and westward-propagating components are filtered out. Contrary, in domain B, a large value for PSD is shown in the eastward-propagating components that amplify with height, and the westward-propagating components are filtered out in the troposphere and stratosphere. At z = 26 km, the waves with zonal wavelengths larger than about 180 km, periods longer than about 3 hrs, and vertical wavelengths ranging from 5 to 13 km are dominant.

3.2. Wave Source and Momentum Flux Spectra

[12] Figure 4 shows power spectrum of the vertical velocity from z = 3 km to the model top and the momentum flux spectrum in the stratosphere with respect to zonal phase speed (c_{px}) in domains A and B. Temporal mean of the background wind (U: thick solid line) is included in all plots, and $U \pm \sigma$, where σ is the standard deviation of U, are also in left panels. The vertical velocity below $z \sim 15$ km, representing the convective forcing, shows a Gaussian-type forcing spectrum with a spectral peak near $c_{px} \approx 0$, although the westward-moving components are somewhat larger (particularly in domain A). In domain A, strong shear of the positive background wind exists from z = 14 to about z = 21 km, and this filters out large fractions of the eastward-propagating waves generated by corresponding wave sources. Consequently, the negative momentum flux is dominant in the stratosphere with its minimum value of -2.44×10^{-4} Nm^{-2} at $c_{px} = -12$ ms^{-1} and z = 17 km. The positive momentum flux is one order of magnitude smaller than the negative momentum flux, with its maximum value of 1.8×10^{-5} Nm^{-2} at c_{px} = 36 ms^{-1} and z = 17 km. On the other hand, in domain B, a relatively weak shear of the negative background wind exists from the surface to the stratosphere, and this filters out most of the westward-propagating waves. As a result, the positive momentum flux is dominant in the stratosphere with its maximum value of 3.8×10^{-4} Nm^{-2} at c_{px} = 12 ms^{-1}, while the minimum momentum flux is -1.9×10^{-5} Nm^{-2} at $c_{px} = -36$ ms^{-1}. These values of the maximum positive and negative momentum fluxes are slightly larger than Chen et al.'s (submitted manuscript, 2005), but in the same order of magnitude. The magnitude of the total momentum flux averaged over z = 17–23 km (2×10^{-3} Nm^{-2} in domain A and 4 $\times$

10^{-3} Nm^{-2} in domain B) also has the same order of magnitude as *Sato* [1993]'s estimate of observed momentum flux using MU radar ($4 \times 10^{-3} \sim 8 \times 10^{-3}$ Nm^{-2}).

[13] The vertical distribution of the momentum flux spectrum can be explained well using the critical-level filtering process, while the decreased magnitude of the momentum flux with height in a non-filtered region is likely due to the damping process. For a westward-propagating wave with a period of 7 hrs and a vertical wavelength of 5 km (Figure 3), it takes about 13 hrs to propagate from z = 17 to 26 km. This is four times larger than the damping time scale of gravity waves with vertical wavelengths less than 10 km, as given by *Marks and Eckermann* [1995]. In addition, the potential wave breaking, which is checked by comparison with the saturation momentum flux given by *Lindzen* [1981], can occur exclusively at near-critical-level phase speeds in the negative momentum flux side (marked by cross).

4. Discussion

[14] In the present simulation, we found that convection in the typhoon-generated cloud bands is the major source of gravity waves and has a nearly symmetric phase-speed spectrum in both eastward- and westward-moving components. However, the induced gravity wave spectrum in the stratosphere is asymmetric mainly due to the critical-level filtering process by the background wind in the troposphere and stratosphere. In a non-filtering region, the decreased magnitude of the momentum flux is likely due to the damping process along with wave breaking, which can occur exclusively near the critical-level phase speeds. This result is somewhat different from that of Chen et al. (submitted manuscript, 2005), who suggested the wave damping as the primary mechanism to explain the vertical distribution of the momentum flux. The discrepancies between the two simulation results may come from several factors, including different typhoon cases occurred at different latitudes, different simulation periods, and particularly different analysis methods. Sensitivity to those factors can be found from ensemble numerical simulations in the future. In the present study, wave propagation in the zonal direction is discussed. Although wave analysis might be better to be done in the wave-propagation direction, it is not straightforward since wave-propagation direction changes with time following the Rusa. Developing a more reasonable way for wave analysis is needed.

[15] Finally, it is noteworthy that gravity waves that reach the upper mesosphere are the eastward-propagating waves, since most of the westward-propagating waves will be filtered out in the upper stratosphere and mesosphere due to the easterly background wind in the summer hemisphere. The positive momentum transport by those eastward-propagating gravity waves in the summer hemisphere is the primary momentum forcing to maintain the wind and temperature in the middle atmosphere general circulation. This implies the importance of convection, including typhoons, as a significant source of gravity waves in the northern hemisphere summertime.

[16] **Acknowledgments.** The authors thank Todd Lane and an anonymous reviewer for their valuable comments on the paper. SYK and HYC were supported by R02-2004-000-10027-0 from the Basic Research Program of the Korea Science and Engineering Foundation (KOSEF) and by the Ministry of Science and Technology of Korea through the National Research Laboratory Program. JJB was supported by the Climate Environment System Research Center sponsored by KOSEF.

References

Alexander, M. J., and J. R. Holton (1997), A model study of zonal forcing in the equatorial stratosphere by convectively induced gravity waves, *J. Atmos. Sci.*, *54*, 408–419.

Chane-Ming, F., G. Roff, L. Robert, and J. Leveau (2002), Gravity wave characteristics over Tromelin Island during the passage of cyclone Hudah, *Geophys. Res. Lett.*, *29*(6), 1094, doi:10.1029/2001GL013286.

Chun, H.-Y., I.-S. Song, J.-J. Baik, and Y.-J. Kim (2004), Impact of a convectively forced gravity wave drag parameterization in NCAR CCM3, *J. Clim.*, *17*, 3530–3547.

Dewan, E. M., R. H. Picard, R. R. O'Neil, H. A. Gardiner, J. Gibson, J. D. Mill, E. Richards, M. Kendra, and W. O. Gallery (1998), MSX satellite observations of thunderstorm-generated gravity waves in mid-wave infrared images of the upper stratosphere, *Geophys. Res. Lett.*, *25*, 939–942.

Dhaka, S. K., M. Takahashi, Y. Shibagaki, M. D. Yamanaka, and S. Fukao (2003), Gravity wave generation in the lower stratosphere due to passage of the typhoon 9426 (Orchid) observed by the MU radar at Shigaraki (34.85°N, 136.10°E), *J. Geophys. Res.*, *108*(D19), 4595, doi:10.1029/2003JD003489.

Dudhia, J. (1989), Numerical study of convection observed during the winter monsoon experiment using a mesoscale two-dimensional model, *J. Atmos. Sci.*, *46*, 3077–3107.

Dudhia, J., D. Gill, K. Manning, W. Wang, C. Bruyere, S. Kelly, and K. Lackey (2003), PSU/NCAR mesoscale modeling system tutorial class note and user's guide: MM5 modeling system version 3, Mesoscale and Microscale Meteorol., Natl. Cent. for Atmos. Res., Boulder, Colo.

Horinouchi, T., T. Nakamura, and J.-i. Kosaka (2002), Convectively generated mesoscale gravity waves simulated throughout the middle atmosphere, *Geophys. Res. Lett.*, *29*(21), 2007, doi:10.1029/2002GL016069.

Kain, J. S., and J. M. Fritsch (1993), *Convective Parameterization for Mesoscale Models: The Kain-Fritsch Scheme. The Representation of Cumulus Convection in Numerical Models*, *Meteorol. Monogr.*, vol. 64, pp. 165–170, Am. Meteorol. Soc., Boston, Mass.

Kwon, H. J., S.-H. Won, M.-H. Ahn, A.-S. Suh, and H.-S. Chung (2002), GFDL-type typhoon initialization in MM5, *Mon. Weather Rev.*, *130*, 2966–2974.

Lane, T. P., M. J. Reeder, and T. L. Clark (2001), Numerical modeling of gravity wave generation by deep tropical convection, *J. Atmos. Sci.*, *58*, 1249–1274.

Lindzen, R. S. (1981), Turbulence and stress owing to gravity wave and tidal breakdown, *J. Geophys. Res.*, *86*, 9707–9714.

Marks, C. J., and S. D. Eckermann (1995), A three-dimensional nonhydrostatic ray-tracing model for gravity waves: Formulation and preliminary results for the middle atmosphere, *J. Atmos. Sci.*, *52*, 1959–1984.

Pfister, L., S. Scott, M. Loewenstein, S. Bowen, and M. Legg (1993), Mesoscale disturbances in the tropical stratosphere excited by convection: Observations and effects on the stratospheric momentum budget, *J. Atmos. Sci.*, *50*, 1058–1075.

Piani, C., D. Durran, M. J. Alexander, and J. R. Holton (2000), A numerical study of three-dimensional gravity waves triggered by deep tropical convection and their role in the dynamics of QBO, *J. Atmos. Sci.*, *57*, 3689–3702.

Sato, K. (1993), Small-scale wind disturbances observed by the MU radar during the passage of Typhoon Kelly, *J. Atmos. Sci.*, *50*, 518–537.

Sato, K., and T. J. Dunkerton (1997), Estimates of momentum flux associated with equatorial Kelvin and gravity waves, *J. Geophys. Res.*, *102*, 26,247–26,261.

Song, I.-S., H.-Y. Chun, and T. P. Lane (2003), Generation mechanisms of convectively forced internal gravity waves and their propagation to the stratosphere, *J. Atmos. Sci.*, *60*, 1960–1980.

J.-J. Baik, School of Earth and Environmental Sciences, Seoul National University, Kwanak-gu, Seoul 151-742, Korea. (jjbaik@snu.ac.kr)

H.-Y. Chun and S.-Y. Kim, Department of Atmospheric Sciences, Yonsei University, 134 Shinchon-dong, Seodaemun-ku, Seoul, 120-749, Korea. (chy@atmos.yonsei.ac.kr; soyoung@atmos.yonsei.ac.kr)